Integrative Biology

Accepted Manuscript

ROYAL SOCIETY OF CHEMISTRY

www.rsc.org/ibiology

Title: Quantitative analysis of resistance to natural killer attacks reveals stepwise killing kinetics

Authors: Paul J. Choi[1*], Timothy J. Mitchison[1]

Affiliations: [1]Department of Systems Biology, Harvard Medical School, Boston, MA 02115, USA
*Corresponding author. Email: paulchoi@post.harvard.edu

ABSTRACT
Molecular mechanisms can protect cancer cells from immune attacks. At the level of bulk tissue, these survival mechanisms are indistinguishable and simply appear as reduced cell death. However, by tracking individual cell survival and death times, we found broad variation in the kinetics of immune evasion. In response to attacks by natural killer cells, we observed that some cancer lines exhibited exponential survival time distributions. Slowly killed cancer lines had reduced exponential rate constants. In contrast, a line engineered to express the serpin protein PI-9, which is known to to promote resistance to immune killing, exhibited a markedly nonexponential survival time distribution. By following the histories of individual cancer cells with multiplexed reporters, we obtained evidence that two or more immune attacks are likely required to kill serpin-expressing cells. Thus, resistance is a finite and measurable quantity, with a distinct kinetic signature. A quantitative model based on independently measured parameters is consistent with our conclusions.

INTRODUCTION
Cytotoxic effector cells in the immune system, including cytotoxic T lymphocytes (CTLs) and natural killer (NK) cells, play an essential role in the control of infections and cancer. However, some potential targets in an infected tissue or cancer may survive immune attack for many reasons. Advantageous genetic mutations in cancer can directly counter cytotoxic mechanisms.[1,2] Isogenic cells can still exhibit varying sensitivities to cytotoxic factors due to varying environments or other factors.[3] Finally, even when all target cells behave identically, the random statistics of killing, which occur unpredictably on a cell-by-cell basis, mean that some cells will survive longer than others purely due to chance.

In cancer, survival mechanisms are multi-faceted and complex.[4] Tumors alter immune responses at a systemic level via tissue interactions,[5] while autonomous mechanisms promote survival at the level of a single cancer cell.[6] In the latter case, individual cancer cells can evade detection by immune cells, and when detected, still resist the ensuing attacks. While a number of molecular mechanisms for evasion and resistance have been identified, understanding their physiological roles in tumors remains a challenging task.

A major pathway for immune-mediated killing of cancer cells involves granzyme B (GzmB), a death-inducing protease that is delivered, usually by CTLs or NK cells, into the cytoplasm of cells targeted for removal.[7,8] A potential means for resisting GzmB activity is the human serine proteinase inhibitor 9 (PI-9), which strongly binds and inhibits GzmB in biochemical assays.[9] Cellular assays suggest that PI-9 may prevent granzyme-mediated death,[10,11,12,13] although there

are conflicting reports.[14] Thus, the finding that PI-9 is overexpressed in certain cancer tissues led to the hypothesis that PI-9 may protect tumor cells from immune attacks.[11, 15]

The physiological role of PI-9 based resistance remains unclear because many factors can determine how a specific biochemical interaction regulates the overall immune-cancer interaction.[16] Even in cell culture models, analysis of PI-9 function has been mainly limited to population measurements at single time points, which provides only a coarse description of survival or death. Instead, we observe and track the fates of single cancer cells during NK attacks, using fluorescent reporters to monitor the outcome of individual NK-cancer interactions. We find that resistant tumor populations exhibit unusual death kinetics that can be explained by multi-step killing from sequential NK attacks. The combination of finite resistance and discrete cytotoxic attacks results in distinct features in the regulation of death at the level of both individual cells and whole populations.

RESULTS

Imaging death in GzmB resistant cells

We used an *in vitro* model for assessing the survival of individual target cells from immune attack. HeLa and MCF7 cell lines stably expressing a biosensor for GzmB sensitively and specifically report attacks by natural killer (NK) attacks.[17] Briefly, GzmB delivered in a one-to-one fashion by the highly cytotoxic NK92-MI cells, an NK line, rapidly leads to a GzmB-positive signal in target cells (Figure 1A). GzmB signals are rapidly followed by cell death.[17]

We modified the HeLa line stably expressing the GzmB reporter, designated HeLa-WT, to overexpress PI-9. After delivery of PI-9 cDNA with a lentivirus and selection for survival against NK cytoxicity, we isolated a clone, designated HeLa-PI9, stably expressing PI-9. Expression of PI-9 in HeLa-PI9 was comparable to the levels present in NK92-MI (Figure 1B). Initial imaging showed that fewer HeLa-PI9 cells were GzmB positive, compared to HeLa-WT cells, after similar incubations with NK92-MI cells (Figure 1C), indicating that PI-9 expression conveyed a GzmB resistant phenotype. Subsequent quantitation showed a strong dependence of resistance on the NK:target ratio (Figure 1D), with protection by PI-9 overexpression most pronounced at low NK:target ratios. Cell death, measured by membrane permeabilization, was almost always preceded by GzmB activation in HeLa-PI9, indicating that prevention of GzmB activation likely prevented cell death during the observation time (Figure 1E and legend).

Measurement of single-cell survival times during NK-mediated killing

To compare the killing kinetics of HeLa-WT versus HeLa-PI9 cells, we measured survival times of individual target cells when co-cultured with different NK cell numbers for 13 hours. Target cells were plated to confluency, with a total of 20,000 cells per well of a 96-well plate. Each well also contained up to 60,000 NK92-MI cells, with almost all targets being killed at the highest NK cell numbers after long times. The survival time is recorded as the time of cell death, as indicated by the GzmB reporter and rapid changes in cell morphology. Accurately recording every target cell's survival time is difficult when many target cells are already killed, because large numbers of corpses obscure the imaging of surviving target cells. To ensure representative survival time

statistics across the entire killing process, we diluted the fluorescently labeled HeLa targets with a nonfluorescent, reporter-free HeLa line, while keeping the total number of targets per well fixed at 20,000 cells. MCF7 cells were also prepared similarly, except they were plated to confluency at 30,000 cells per well of a 96-well plate, and the NK cell numbers adjusted to the same NK:target ratio. Following preparation of targets, NK cells were added, and automated imaging begun within 10 minutes afterwards to define $t = 0$, continuing for 13 additional hours. The resulting survival times were recorded for at least 300 target cells for each condition.

Figures 2A and 2B show histograms of survival times, $P(T)$, for HeLa-WT and HeLa-PI9 cells when treated with 1:1 or 3:1 NK:target ratios. HeLa-WT survival time histograms were well-fit by single exponential distributions, indicating that killing of HeLa-WT populations can be approximated as single-step processes with rate constants k_{WT}, such that $P_{WT}(T) = k_{WT}\exp(-k_{WT}T)$. For these cases, a simple conceptual model describes the killing process. Each NK-target attack occurs independently, and a single attack is likely to result in rapid target death. Increasing the NK:target ratio increases the rate constant, because the higher frequency of NK-target contacts leads to a higher rate of NK attacks.

Past work found that NK killing does not always adhere to this simple model.[17] We previously observed evidence of non-exponential, bursting kinetics in killing of multiple HeLa-WT and MCF7 targets by single NK cells. The key difference is that our former result occurred in the context of serial killing by NK cells at extremely low NK:target ratios. For NK cells at higher ratios, NK cells are only likely to kill at most one target. Under these conditions, only the rate of the first killing event is relevant. If this rate is identical between NK cells, the results will be exponentially distributed killing kinetics.

In contrast to the HeLa-WT survival times, HeLa-PI9 survival times were peaked at later times, indicating nonexponential kinetics. For comparison, we also measured survival times in the same experiment for an MCF7 target line (Figure 2C), previously shown to be a worse target than HeLa-WT for NK92-MI.[17] MCF7 displays exponential survival time histograms, but with slower rate constants at the same NK doses as HeLa-WT, indicating that NK-MCF7 interactions are less efficient in generating productive NK attacks. However, the nature of the model and the associated kinetics remained the same for MCF7 targets. Although MCF7 lines can overexpress PI-9 under estrogen treatment,[13] under the experimental conditions, MCF7 targets do not express more PI-9 than HeLa-WT (Figure 1B). Thus, the expression of PI-9 uniquely alters the survival time kinetics, not by simply changing the rate constant, but by changing the structure of the survival time histograms.

Evidence for multiple hits via calcium imaging

Nonzero peaked distributions indicate that HeLa-PI9 killing is poorly approximated by a single step process. Multiple steps would naturally arise if more than one NK attack was necessary to kill the resistant line. We therefore imaged HeLa-WT or HeLa-PI9 cells stably expressing the calcium reporter R-GECO1[18] to test if multiple hits are necessary for death in HeLa-PI9. Direct detection of multiple attacks is not possible with the GzmB reporter, because if PI-9 in the target cell completely inhibits the GzmB introduced by the first attack, the reporter will show no change until the second attack. However, calcium transients are expected from an NK attack

even if GzmB is inactive because of perforin, a pore-forming protein delivered alongside GzmB by NK cells. By perforating the cell membrane and triggering a temporary rise in cytoplasmic calcium ion levels, perforin triggers the uptake of extracellular GzmB by target cells.[19]

Initial calcium imaging experiments were complicated by near-simultaneous transients in clusters of neighboring cells. Calcium transients presumably spread from a cell subjected to an NK attack to neighbors by paracrine signaling and/or gap junctions.[20] Cell-cell communication was therefore minimized by sparse plating of target cells and addition of apyrase to the medium to deplete extracellular ATP, a common paracrine signal that elicits calcium transients. The use of apyrase to quench paracrine calcium signaling has been previously demonstrated.[20] Under these conditions, calcium transients were almost always restricted to single cells, and no transients were observed in the absence of NK cells.

In HeLa-WT targets, a single train of calcium transients always preceded a rapid increase in GzmB activity by at least several minutes (Figure 3A). No transients were observed in HeLa-WT targets in the absence of GzmB activity or NK treatment. However, in HeLa-PI9 targets (Figures 3B and 3C), the pattern of calcium transients showed greater variation, and depended on the final target state. For HeLa-PI9 targets that survived the 12 hours of co-incubation with NK cells (Figure 3B), single or brief trains of calcium transients were frequently observed, along with no change in the GzmB reporter's signal. For HeLa-PI9 targets that were killed by NK cells (Figure 3C), multiple trains of calcium transients were frequently observed, along with a slow change in the GzmB reporter's signal after the later calcium transients. Because of the variation in the precise number, timing, and magnitude of calcium transients, we did not directly equate each train of calcium transients with individual NK attacks. Thus, a quantitative analysis of single-cell behavior was not applicable in this case. Nevertheless, the appearance of multiple trains of calcium transients in killed targets and the appearance of single trains of calcium transients in surviving targets supports the conclusion that HeLa-PI9 targets can survive single NK hits, but succumb to multiple NK attacks.

A simple model is consistent with single-cell kinetics and population dynamics

We compared our data to simple quantitative models describing the killing process. A general kinetic scheme of resistance and death is shown at the top of Figure 4, with hit rates k_{Ai} corresponding to the rate of NK hits and death rates k_{Di} corresponding to the rate of a death process following a specific hit. A single hit corresponds to a single round of GzmB release and cytotoxic attack. Different biological models of killing can be evaluated by applying different constraints to the k_{Ai} and k_{Di} values. In all cases, we make the assumption that individual substeps have exponentially distributed waiting times.

To focus our analysis, we first obtained additional experimental data to restrict ourselves to biologically relevant models. To restrict the first hit rate, k_{A1}, we measured the time to the first observable calcium transient for HeLa-WT and HeLa-PI9 cells identically treated with NK cells in the same experimental run. We observed mean times of 51 ± 6 and 48 ± 9 minutes (standard errors, n = 36) for HeLa-WT and HeLa-PI9 cells, respectively, indicating that k_{A1} is similar for both cases, even though HeLa-PI9 cells died at a much slower rate. This data supports the assumption that the rate of NK attacks against HeLa-PI9 is identical to the rate of attacks against

HeLa-WT, because the external state of the cell is unlikely to be changed by cytoplasmic PI9 expression. Thus, we set $k_{A1} = k_{WT}$ for all models.

Similarly, we could restrict the values of k_D from the calcium imaging data. For example, following successful NK attacks, activation of GzmB and subsequent death is clearly a slower process in HeLa-PI9 targets, compared to HeLa-WT targets. Thus, the death rate, k_{Di}, in Figure 4, is likely to have a slow, appreciable value, and there must exist i such that $0 < k_{Di} < 0.17$ min^{-1}, where the upper limit is given by the fact that the changes are slower than the microscopy frame rate. Because it is not possible to determine which of the calcium transients in Figure 3C corresponds to the NK attack that triggers death, the values of k_{Di} cannot be determined directly. We were able, however, to set bounds on the kinetics of cell death in HeLa-PI9 targets by measuring the time between the first calcium transient and an observable GzmB reporter change, which we term ΔT_D. The first attack must correspond to the first calcium transient, but given the variable nature of the calcium response, the timing of subsequent attacks is not precisely known. If we assume HeLa-PI9 targets are killed after exactly n attacks, $\Delta T_D = (\sum_{i=1..n} 1/k_{Ai}) + 1/k_{Dn}$. While $(\sum_{i=1..n} 1/k_{Ai})$ is dependent on the number of NK cells present, we assume that k_{Dn} is independent of the NK number as long as all NK attacks occur within less than one cell cycle. Then, $\Delta T_D \geq 1/k_{Dn}$, with $\Delta T_D \approx 1/k_{Dn}$ for sufficiently large k_{Ai} values. By adding a large excess of NK cells (> 4:1 NK:target), we experimentally minimize $1/k_{Ai}$ by maximizing the rate of NK attacks. In this case, we measured $\Delta T_D = 116 \pm 17$ min (standard error, $n = 20$). Then, we can set a bound of $k_{Dn} \geq 0.0087$ min^{-1} for a model in which targets are killed after exactly n attacks.

As further criteria, a single type of model should fit both doses of NK treatment, although the lower NK dose treatment had weaker discriminatory power because of noise at lower total levels of killing. Additionally, the rate of death after an NK attack should be independent of the NK dose, since the internal death program, once initiated, is unlikely to be changed by external factors.

Using these experimental criteria and the data in Figure 2, we considered several models, and asked which of these models was consistent with all of the experimental data. To begin, we tested models where all NK attacks had identical rates, such that all nonzero $k_{Ai} = k_{WT}$. This approach, while not comprehensive, provides a simple quantitative survey of some relevant models. Models corresponding to exactly one, two, or three hits per kill are shown in Schemes 1-3 of Figure 4. Scheme 4 shows the case where every hit has an identical probability of death.

In Scheme I, the death rate, as the sole free parameter, is uniquely determined by the mean survival time, as measured in Figure 2. The p-value of the corresponding fit is moderate (see Table 1 for all parameter values), and the values of k_{D1} fail to meet the criteria of $k_{D1} \geq 0.0087$ min^{-1}. In conjunction with the extended calcium transients observed in Figure 3 for HeLa-PI9, we conclude that killing induced by exactly one hit is unlikely to explain the observed data.

In Scheme II, the model cannot be confidently rejected based on the p-value of the fit alone, and the values of $k_{D2} = 0.150$ min^{-1} and 0.103 min^{-1} at 1:1 and 3:1 NK:target ratios, respectively, satisfy the criteria of $k_{D2} \geq 0.0087$ min^{-1}. Directly inserting the bound, $k_{D2} = 0.0087$ min^{-1}, for both NK:target ratios also provides reasonable fits (see Table 1). Thus, this scheme satisfies all

of the previously stated criteria, and we conclude that a model of killing induced by exactly two identical hits and a slow death process is consistent with the observed data.

Scheme III is unlikely, as the sum of three identical steps with rate k_{WT} is greater than the observed mean survival time. Thus, we conclude that killing induced by exactly three identical hits is unlikely to explain the observed data.

Scheme IV has a very small *p*-value, and the value of k_D also fails to meet the minimum criteria. Thus, killing induced with the same probability by every hit is unlikely to explain the observed data.

Thus, while other models with arbitrary structures and parameters may also be consistent with the data, the model of two identical NK hits followed by slow killing is a parsimonious, biologically feasible model that agrees with all of the experimental observations. More importantly, models based on single-hit killing are unlikely to agree with all of the experimental observations.

DISCUSSION

We found that NK killing of cancer targets in cell culture models is consistent with simple kinetic schemes. Killing of HeLa-WT and naturally less susceptible MCF7 targets followed exponential kinetics. Killing of resistant HeLa-PI9 targets, in contrast, followed multi-step kinetics, with more than one hit required to kill most targets. The multi-hit hypothesis for killing PI9 expressing cells was demonstrated by killing kinetics (Figure 2B), calcium imaging (Figure 3), and fitting to a multi-hit model (Figure 4). Exponential killing kinetics for sensitive targets have been previously observed in pre-formed CTL-target conjugates,[21] but our work shows that the entire process of NK motility, recognition, and degranulation can be summarized by a single exponential parameter. In addition, past models of tumor killing[22] have been evaluated using bulk lysis assays, which are imprecise approximations of NK attack rates. By observing the statistics of NK attacks and death for individual target cells, we more directly and sensitively evaluated kinetic models of killing. As mentioned above, very low NK:target ratios lead to bursts of serial killing rather than exponential kinetics.[17]

The killing kinetics show, at the level of single-cell actions, that targets can resist NK attacks by more than one mechanism. Compared to the susceptible HeLa line, MCF-7 cells resist by slower kinetics of a single hit kill, while HeLa-PI9 resist by requiring multiple hits. Past models of NK or related CTL killing[23,24] implicitly assumed a “one-hit, one-kill” hypothesis, such that a single immune attack results in deterministic and irreversible target death. No alternative models have been previously demonstrated. However, our finding that multiple attacks are required to kill HeLa-PI9 targets suggests that alternatives to the “one-hit, one-kill” scenario do exist. Importantly, the resistance conferred by PI-9 overexpression is kinetically distinct from other strategies of immune escape. MCF7 targets have reduced killing compared to HeLa-WT, but MCF7 targets still display exponential killing kinetics. MCF7 targets may be recognized less efficiently by NK cells but still adhere to the “one-hit, one-kill” scenario.

An important future question is how kinetic principles and resistance mechanisms derived from simplified *in vitro* models are relevant to NK-tumor interactions in the much more complex environment of tumors. Whether cytotoxic cells commonly exhibit exponential or bursting serial killing kinetics, and whether single attacks or multiple attacks are necessary to kill real targets, are fundamental questions relevant to transplant rejection as well as tumor immunosurveillance. It may be possible to address these questions by intravital imaging in mouse models. In tumors, the probability of a single NK cell attacking the same target twice may be very low, due to the properties of diffusive searches in three dimensions. Then, appreciable killing would only take place at high NK densities, such that multiple NK cells can attack the same target. Treatments such as cytokine therapy[25] and adoptive cellular therapy[26] can greatly boost NK densities beyond endogenous levels.[27,28,29] One question is how the efficacy of such treatments depends on the altering the kinetics of individual cell-cell interactions. Thus, kinetic principles in basic systems can still motivate future analysis or interpretation of more complex systems.

MATERIALS AND METHODS

Plasmids and cell lines

The construction and propagation of HeLa-WT, MCF7, and NK92-MI cells was described previously (Choi). The use of properly maintained and/or low passage NK92-MI cells was essential for highest activity and exponential kinetics. We note that poor passaging techniques would result in irreversibly reduced activity and perturbed kinetics even against HeLa-WT targets. The cDNA for PI-9 (Open Biosystems, Clone ID# 3140427) was transferred to the lentiviral backbone pHR-CMV-IRES-hygro generated by excision of the insert with BamHI/XhoI digestion from Addgene plasmid 23135. The HeLa-PI9 cell line was constructed by infection with the resulting plasmid and clonal selection. Construction of the R-GECO1 reporter line from HeLa-WT has been previously reported,[17] and the same construction was applied to HeLa-PI9.

Microscopy

Imaging was performed as previously described,[17] using identical filter sets and objectives, with the addition of an RFP filter set (Chroma) being used for R-GECO1 or Sytox Orange imaging when appropriate. Time-lapse movies were recorded with a frame interval of 30 seconds for calcium imaging and 6 minutes for survival time data.

Data analysis and modeling

Image processing was performed using NIS Elements software. For construction of single-cell time traces, the average fluorescence intensity within a 3x3 bin was recorded for all optical channels for a single cell, using the tracking module in NIS Elements, with manual correction of tracking errors. Background intensities were also recorded in regions free of cells. After background subtraction, the appropriate channels were ratioed, to give the GzmB and calcium transient activities. The timing of death events were identified manually based on activation of GzmB and morphology changes. Clear identification of GzmB activation was possible after less than 20% of the maximal change (see Figure 3, which shows the maximal change in ideal cases for HeLa-WT). Sharp morphology changes occurred during the passage of one frame to the next.

Kinetic schemes were evaluated using Python scripts. At most one parameter was unknown for each scheme, such that it could be calculated directly from the mean of the survival time distribution and other imposed constraints, such as the structure of the model and rates set at "infinity". Because the experimental observations occur over a finite time, the unknown parameter was not calculated using integrated, closed-form expressions. Instead, the parameter value was varied and simulated data ($n > 10^5$) generated from the corresponding model over the finite observation time. The mean of the simulated data was calculated as a function of the input parameter value, and then matched to the observed mean of the survival time distribution to determine the parameter value.

ACKNOWLEDGEMENTS
We thank N. Georgoulia and other members of the Mitchison lab for technical assistance and discussions, J. Waters and the staff of the Nikon Imaging Center at Harvard Medical School for assistance with microscopy, J. Paulsson for discussions, and J. Tallarico and Y. Feng for additional support. This work is supported by a collaborative arrangement with the Novartis Institutes for Biomedical Research.

REFERENCES

1. H. F. Igney, P. H. Krammer, *Nat Rev Cancer*, 1993, **2**, 277-288.

2 J. Hasenkamp, A. Borgerding, G. Wulf, M. Uhrberg, W. Jung, S. Dingeldein, L. Truemper, B. Glass, *Scand J Immunol,* 2006, **64**, 444-449.

3. S. L. Spencer, S. Gaudet, J. G. Albeck, J. M. Burke, P. K. Sorger, *Nature*, 2010, **459**, 428-432.

4. T. L. Whiteside, *Seminars in Cancer Biology*, 2006, **16**, 3-15.

5. A. Sica, V. Bronte, *J Clin Invest*, 2007, **117**, 1155-1166.

6. Q. L. Deveraux, J. C. Reed, *Genes Dev*, 1999, **13**, 239-252.

7. D. Chowdhury, J. Lieberman, *Ann Rev Immnunol*, 2008, **26**, 389-420.

8. S. P. Cullen, M. Brunet, S. J. Martin, *Cell Death Differ*, 2010, **17**, 616-623.

9. J. Sun, C. H. Bird, V. Sutton, L. McDonald, P. B. Coughlin, T. A. De Jong, J. A. Trapani, P. I. Bird, *J Biol Chem*, 1996, **271**, 27802-27809.

10. C. H. Bird, V. R. Sutton, J. Sun, C. E. Hirst, A. Novak, S. Kumar, J. A. Trapani, P. I. Bird, *Mol Cell Biol*, 1998, **18**, 6387-6398.

11. J. P. Medema, J. de Jong, L. T. Peltenburg, E. M. Verdegaal, A. Gorter, S. A. Bres, K. L. Franken, M. Hahne, J. P. Albar, C. J. Melief, R. Offringa, *Proc Natl Acad Sci USA*, 2001, **98**, 11515-11520.

12. T. D. Cunningham, X. Jiang, D. J. Shapiro, *Cell Immunol*, 2007, **245**, 32-41.

13. X. Jiang, S. J. Ellison, E. T. Alarid, D. J. Shapiro, *Oncogene*, 2007, **26**, 4106-4114.

14. R. Godal, U. Keilholz, L. Uharek, A. Letsch, A. M. Asemissen, A. Busse, I.-K. Na, E. Thiel, C. Scheibenbogen, *Blood*, 2006, **107**, 3205-3211.

15. B. A. Bladergroen, C. J. Meijer, R. L. ten Berge, C. E. Hack, J. J. Muris, F. Dukers, A. Chott, Y. Kazama, J. J. Oudejans, O. van Berkum, J. A. Kummer, *Blood*, 2002, **99**, 232-237.

16. M. Bots, R. Offringa, J. P. Medema, *Blood*, 2006, **107**: 4974-4975.

17. P. J. Choi, T. J. Mitchison, *Proc Natl Acad Sci USA*, 2013, **110**, 6488-93.

18. Y. Zhao, S. Araki, J. Wu, T. Teramoto, Y. F. Chang, M. Nakano, A. S. Abdelfattah, M. Fujiwara, T. Ishihara, T. Nagai, R. E. Campbell, *Science*, 2011, **333**, 1888-1891.

19. J. Thiery, D. Keefe, S. Saffarian, D. Martinvalet, M. Walch, E. Boucrot, T. Kirchhausen, J. Lieberman, *Blood*, 2010, **115**, 1582-1593.

20. K. Paemeleire, P. E. Martin, S. L. Coleman, K. E. Fogarty, W. A. Carrington, L Leybaert, R. A. Tuft, W. H. Evans, M. J. Sanderson, *Mol Biol Cell*, 2000, **11**, 1815-1827.

21. E. A. Grimm, J. A. Thoma, B. Bonavida, *J Immunol*, 1979, **123**, 2870-2877.

22. L. G. de Pillis, A. E. Radunskaya, C. Wiseman, *Cancer Res*, 2005, **65**, 7950-7958.

23. A. S. Perelson, G. I. Bell, *J Immunol*, 1982, **129**, 2796-2801.

24. R. R. Regoes, A. Yates, R. Antia, *Immunol Cell Biol*, 2007, **85**, 274-279.

25. P. A. Albertsson, P. H. Basse, M. Hokland, R. H. Goldfarb, J. F. Nagelkerke, U. Nannmark, P. J. Kuppen, *Trends Immunol*, 2003, **24**, 603-609.

26. P. Basse, R. B. Herberman, U. Nannmark, B. R. Johansson, M. Hokland, K. Wasserman, R. H. Goldfarb, *J Exp Med*, 1991, **174**, 479-488.

27. S. Ishigami, S. Natsugoe, K. Tokuda, A. Nakajo, X. Che, H. Iwashige, K. Aridome, S. Hokita, T. Aikou, *Cancer*, 2000, **88**, 577-583.

28. I. Takanami, K. Takeuchi, M. Giga, *J Thorac Cardiovasc Surg*, 2001, **121**, 1058-1063.

29. F. R. Villegas, S. Coca, V. G .Villarrubia, R. Jiménez, M. J. Chillón, J. Jareño, M. Zuil, L. Callol, *Lung Cancer*, 2002, **35**: 23-28.

FIGURES LEGENDS

Figure 1. Live-cell reporter for GzmB killing and resistance.
(A) Summary of GzmB biosensor. Fluorescence resonance energy transfer (FRET) between a cyan (CFP) and yellow (YFP) fluorescent protein is abolished after specific cleavage of the linker peptide by GzmB transferred from the NK cell to target cell. (B) PI-9 expression in the constructed HeLa-PI9 line is comparable to the PI-9 expression in the NK line NK92-MI. (C) GzmB biosensor activation. HeLa-WT or HeLa-PI9 cells stably expressing the GzmB reporter were co-incubated with unlabeled NK92-MI cells. White targets cells turn blue upon NK attack and subsequent GzmB activity. (D) The fraction of GzmB positive target cells after 6 hours was determined at different NK:target ratios using experimental conditions identical for the data in Figure 2. (E) GzmB activity precedes cell lysis. HeLa targets are co-incubated with NK92-MI cells and 0.5 μM of the membrane impermeable DNA stain Sytox Orange. GzmB activity, indicated by the blue cells, is followed by membrane permeabilization, indicated by the red overlay. In a typical experiment over 6 hours of imaging, such that at least half the targets are dead, 25/25 HeLa-WT and 25/25 HeLa-PI9 cells that display GzmB activity are followed by membrane permeabilization. In the same experiment, 0/25 HeLa-WT and 1/25 HeLa-PI9 cells that do not display GzmB activity show membrane permeabilization, indicating that, as expected, PI-9 overexpression likely inhibits killing by interfering with GzmB activity, and that eventual death is still GzmB-dependent.

Figure 2. Survival time histograms during NK killing.
Survival time histograms indicate the distribution of death times for individual HeLa-WT (A), HeLa-PI9 (B), or MCF7 (C) target cells treated with two concentrations of NK92-MI cells. The experimental conditions are described in the text. The total numbers of cells analyzed for each case is given by *n*. Observed histograms are shown as gray circles and calculated distributions are shown as a black line. The solid lines are not parameter-optimized fits. Rather, they are superimposed mathematical functions. For HeLa-WT and MCF7 cells, single exponential distributions were calculated from the mean of the observed distribution. The corresponding *p*-values, calculated as described in Table 1, indicate that the models cannot be rejected as an explanation for the observed data. The rate constants for HeLa-WT at 1:1 NK:target, HeLa-WT at 3:1 NK:target, MCF7 at 1:1 NK:target, and MCF7 at 3:1 NK:target are 0.0042 min^{-1}, 0.0084 min^{-1}, 0.0022 min^{-1}, and 0.0046 min^{-1}, respectively. For HeLa-PI9, distributions were calculated assuming the same NK attack rates as for HeLa-WT, but requiring two successive attacks and a slow death rate of 0.0086 min^{-1}. See the text for additional details. The distribution corresponds to a triple convolution of exponential distributions, each with their respective rate constant.

Figure 3. Calcium transients in target cells provide evidence of multiple NK attacks.
HeLa-WT or HeLa-PI9 targets dual labeled with both the GzmB yellow-blue reporter and the R-GECO1 red calcium reporter were plated sparsely at 1000 cells per well of a 96 well plate and co-incubated with 1000-4000 NK92-MI cells for 6 hours with 40 units/mL apyrase. Single-cell profiles for GzmB activity (gray) and calcium transients (black) are shown for dying HeLa-WT targets (A), surviving HeLa-PI9 targets (B), and dying HeLa-PI9 (C) targets. After background subtraction, GzmB activity is calculated by the ratio of the blue (CFP) emission to resonance transfer (FRET) emission, whereas calcium levels are calculated as the ratio of the red (RFP) emission to yellow (YFP) emission. Dying HeLa-WT and surviving HeLa-PI9 targets exhibit a

single or small number of calcium transients, while large numbers of calcium transients precede death of HeLa-PI9 targets.

Figure 4. Modeling the kinetics of NK killing for resistant target populations.
At the top is a generalized kinetic scheme for NK attacks and subsequent death in resistant HeLa-PI9. Choosing different values of k_{Ai} and k_{Di}, such as setting rates to be zero, results in models corresponding to different biological scenarios. The mean of each model distribution is set to equal the mean of the observed experimental distribution, which uniquely pre-determines all parameter values for the schemes tested, as shown where appropriate for each scheme. See the main text for more details. Example schemes are shown, including delayed death by a single (I), two (II), or three (III) NK attacks, and a memoryless death process (IV). See Table 1 for exact parameter values and the main text for further model criteria.

TABLES

NK dose	Scheme[a]	*p*-value[b]	χ^2	k_{A1}[c]	k_{A2}	k_{A3}	k_{A4+}[d]	k_{D1}	k_{D2}	k_{D3}	k_{D4+}[d]
1:1	I	1.0	78	0.0042				0.0023			
3:1	I	0.30	85	0.0084				0.0039			
1:1	II	1.0	117	0.0042	0.0042			0	0.0150		
3:1	II	1.0	59	0.0084	0.0084			0	0.0103		
1:1	II[f]	1.0	106	.0042	.0042			0	.0087		
3:1	II[f]	1.0	61	.0084	.0084			0	.0087		
1:1	III[g]	NA	NA	0.0042	0.0042	0.0042		0	0	NA	
3:1	III[g]	NA	NA	0.0084	0.0084	0.0084		0	0	NA	
1:1	IV	$<10^{-4}$	6024	0.0042	0.0042	0.0042	0.0042	$3x10^{-5}$	$3x10^{-5}$	$3x10^{-5}$	$3x10^{-5}$
3:1	IV	$<10^{-4}$	169	0.0084	0.0084	0.0084	0.0084	0.0020	0.0020	0.0020	0.0020

Table 1. Numerical values used in model calculations

[a] Corresponding scheme from Figure 4.

[b] *p*-values are calculated by simulating 10^4 data sets from the model distribution with an identical sample size and observation time as the experimental observation. For each simulated data set, χ^2 is determined by comparison with the model's predicted distribution values. The null hypothesis is that the experimental observation results from the same model. Calculating χ^2 for the experimental observation and comparison with the rank-ordered set of 10^4 χ^2 values yields a *p*-value. At small values of the *p*-value, we reject the null hypothesis, and accordingly, the model as an explanation for the observations.

[c] All rate constants are in units of min^{-1}. All rates not explicitly stated are equal to 0.

[d] Rate for all further steps are identical to this value.

[e] HeLa-WT rate constants were experimentally determined to be 0.0042 min^{-1} and 0.0084 min^{-1} at 1:1 and 3:1 NK:target ratios, respectively. These measured HeLa-WT values are substituted for the rate of NK attacks the scenarios listed in this table and in Figure 4.

[f] Follows scheme II but uses the value of k_{D2} determined from calcium imaging.

[g] Sum of the first 3 steps already approaches or exceeds the mean observed survival time such that the model was rejected.

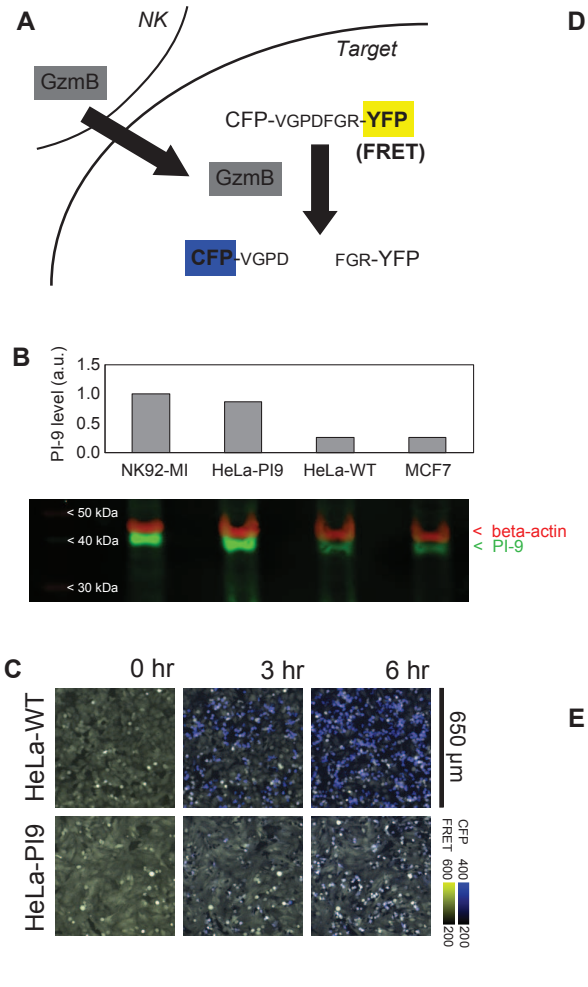

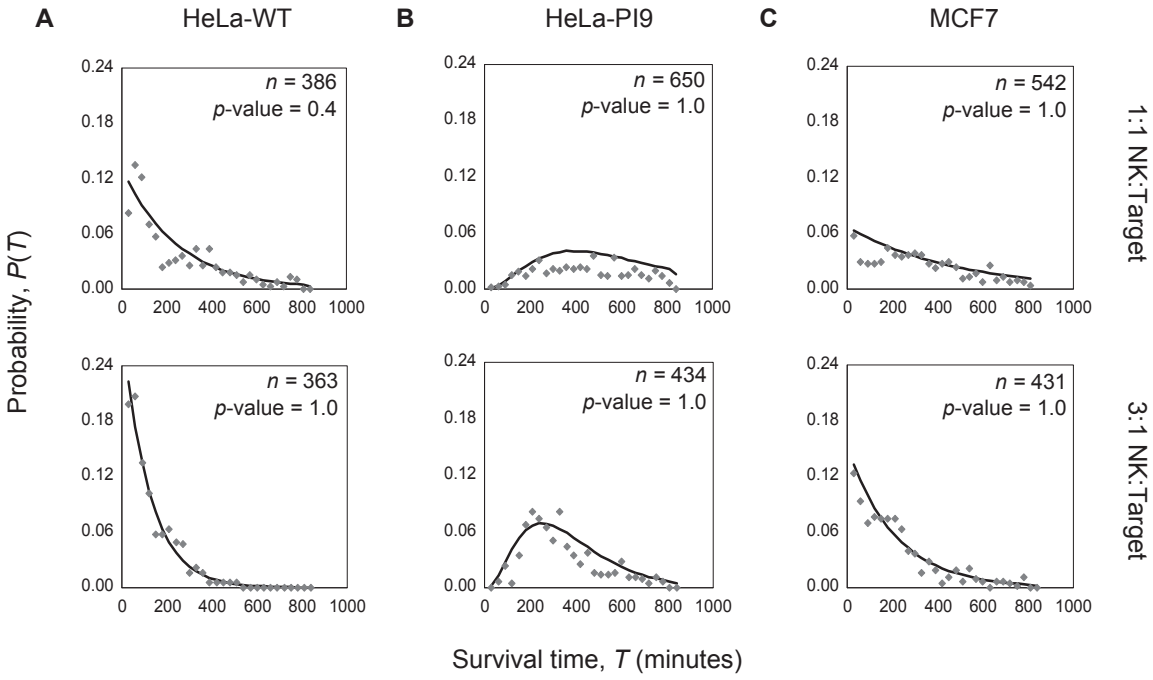

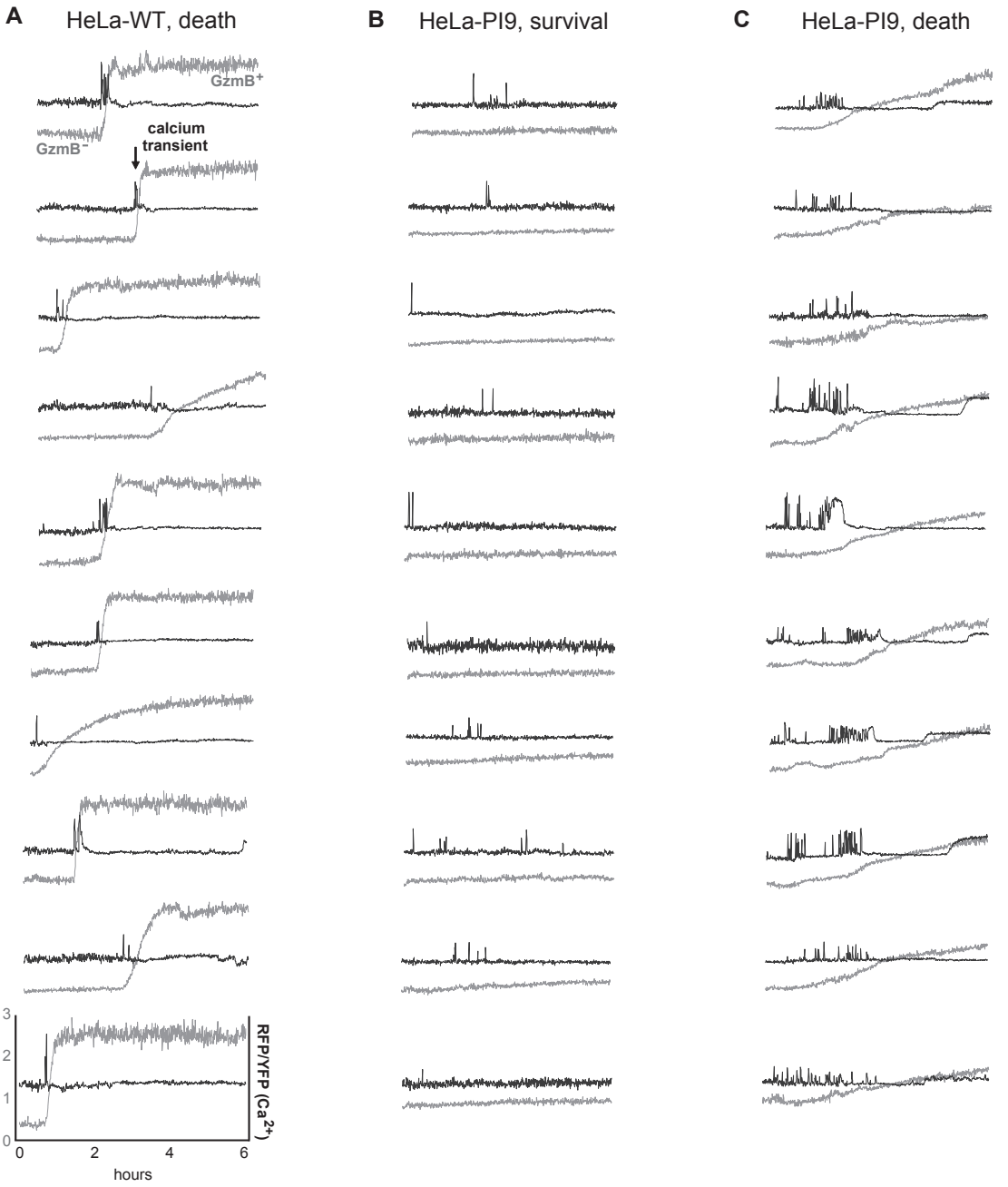

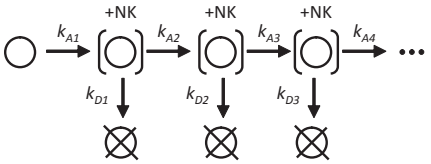

◯ = target cell
k_{Ai} = rate of i^{th}NK attack
k_{Di} = rate of death after i^{th}attack
k_{WT}= rate of NK attack in HeLa-WT
T_{ave}= mean survival time of HeLa-PI9

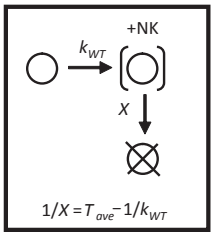

I

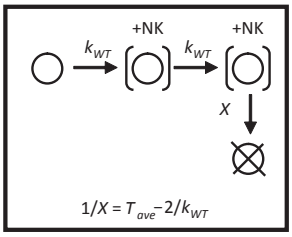

II

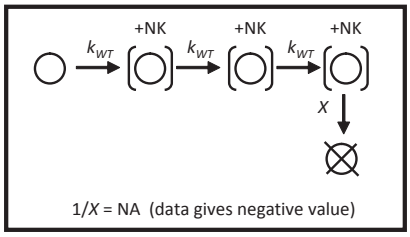

III

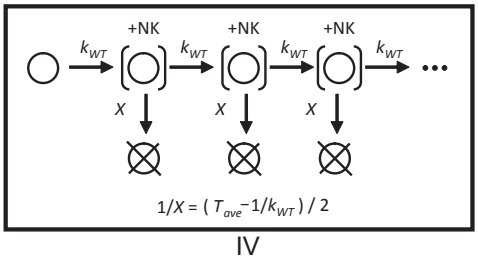

IV